

What controls the seasonal cycle of columnar methane observed by GOSAT over different regions in India.

Naveen Chandra^{1*}, Sachiko Hayashida¹, Tazu Saeki², and Prabir K. Patra²

¹ Nara Women's University, Kita-Uoya Nishimachi, Nara 630-8506, Japan

² Department of Environmental Geochemical Cycle Research, JAMSTEC, Yokohama 2360001, Japan

Correspondence to: Naveen Chandra (nav.phy09@gmail.com)

Abstract. Methane (CH_4) is one of the most important short-lived climate forcers for its critical roles in greenhouse warming and air pollution chemistry in the troposphere, and water vapor budget in the stratosphere. It is estimated that up to about 8% of global CH_4 emissions occur from South Asia, covering less than 1% of global land. With the availability of satellite observations from space, variability in CH_4 have been captured for most parts of the global land with major emissions, which were otherwise not covered by the surface observation network. However, satellite observations of the columnar dry-air mole fractions of methane (XCH_4) do not allow us to derive emission information straightforwardly, unlike in-situ measurements near the source region, without separating the role of transport and chemistry. XCH_4 is an integrated measure of CH_4 densities at all altitudes from surface to the top of the atmosphere. Here, we present an analysis of XCH_4 variability over different parts of India and the surrounding cleaner oceanic regions as measured by Greenhouse gases Observation SATellite (GOSAT) and simulated by an atmospheric chemistry-transport model (ACTM). Distinct seasonal variations of XCH_4 have been observed over the northern (north of 15°N) and southern part (south of 15°N) of India, corresponding to the peak during southwest monsoon (July-September) and early autumn season (October-December), respectively. Analysis of the transport, emission and chemistry contributions to XCH_4 using ACTM suggests that distinct XCH_4 seasonal cycle over northern and southern regions of India is governed by the both heterogeneous distributions of surface emissions and contribution of partial CH_4 column in the upper troposphere. Over most part of the northern Indian Gangetic Plain regions, up to 40% of the peak during the southwest (SW) monsoon season is attributed to the lower troposphere (~ 1000 -600 hPa), while $\sim 40\%$ to uplifted high- CH_4 air masses in the upper troposphere (~ 600 -200 hPa). In contrast, XCH_4 seasonal enhancement over the semi-arid western India is attributed mainly ($\sim 70\%$) to the upper troposphere. The seasonal cycle of XCH_4 over the southern peninsula and oceanic region is contributed up to 60% by the lower tropospheric region. These differences arise due to the complex atmospheric transport mechanisms, caused by the seasonally varying monsoon. The CH_4 enriched air mass is uplifted from high emission region of the Gangetic Plain by the SW monsoon circulation and deep cumulus convection, and then confined by anticyclonic wind in the upper tropospheric heights (~ 200 hPa). The anticyclonic confinement of surface emission over a wider South Asia region leads to strong contribution of the upper troposphere in formation of the XCH_4 peak over most regions in northern India, including the semi-arid regions with extremely low CH_4 emissions. Based on this analysis, we suggest that a link between surface emissions and higher levels of XCH_4 is not always valid over Asian monsoon regions, although there is often a fair correlation between surface emissions and XCH_4 . The overall validity of ACTM simulation for capturing GOSAT observed seasonal and spatial XCH_4 variability will allow us to perform inverse modelling of XCH_4 emissions in the future using XCH_4 data.

1. Introduction

Methane (CH₄) is the second most important anthropogenic greenhouse gas (GHG) after carbon dioxide (CO₂) and accounts for ~20% (+0.97 W m⁻²) of the increase in total direct radiative forcing, since 1750 (Myhre et al., 2013). CH₄ is emitted from a range of anthropogenic and natural sources on the Earth's surface into the atmosphere. The main natural sources of CH₄ include wetlands and termites (Matthews and Fung, 1987; Cao et al., 1998; Sugimoto et al., 1998). Livestock, rice cultivation, fossil fuel industry (production and uses of natural gas, oil and coal) and landfills are the major sectors among the anthropogenic sources (Crutzen et al., 1986; Minami and Neue, 1994; Olivier et al., 2006; Yan et al., 2009). These results also suggest that the Asia region is emission hotspot of CH₄ due to large number livestock, intense cultivation, coal mining, waste management and other anthropogenic activities (EDGAR2FT, 2013).

With a short atmospheric lifetime of about 10 years (e.g., Patra et al., 2011a) and having 34 times more potential to trap heat than CO₂ on mass basis over a 100-year timescale (IPCC AR5), mitigation of CH₄ emissions could be the most important way to limit global warming at inter-decadal time scales (Shindell et al., 2009). Better knowledge of CH₄ distribution and quantification of its emission flux is indispensable for assessing possible mitigation strategies. However, sources of CH₄ are not yet well quantified due to sparse ground based measurements, which results in limited representation on a larger scale (Dlugokencky et al., 2011; Patra et al., 2016). Recent technological advances have made it possible to detect spatial and temporal variations in atmospheric CH₄ from space (Frankenberg et al., 2008; Kuze et al., 2009), which could fill the gaps left by ground, aircraft and ship-based measurements, albeit at a lower accuracy than the *in situ* measurements. Further, despite the satellite observations having an advantage of providing continuous monitoring over a wide spatial range, the information obtained from passive nadir-sensors that use solar radiation at Short-Wavelength Infrared (SWIR) spectral band, is limited to columnar dry-air mole fractions of methane (XCH₄). This is an integrated measure of CH₄ with contributions from the different vertical atmospheric layers, i.e., from the measurement point on the Earth's surface to the top of the atmosphere (up to about 100km or more precisely to the satellite orbit).

The Indian region exerts a significant impact on the global CH₄ emissions, with 37±3.7 Tg-CH₄ of about 500 Tg-CH₄ during the 2000s is emitted from the South Asia region consisting of India, Pakistan, Bangladesh, Nepal, Bhutan and Sri Lanka (Patra et al., 2013). The Indo-Gangetic Plain (IGP), located in the foothills of the Himalayas, is one of the most polluted regions in the world, hosts 70% of coal-fired thermal power plants in India and experience intense agricultural activity (Kar et al., 2010). This region is of particular interest mainly due to the coexistence of deep convection and large emission of pollutants (including CH₄) from a variety of natural and anthropogenic sources. Rainfall during the SW monsoon season cause higher CH₄ emissions from the paddy fields and wetlands (e.g., Matthews and Fung, 1987; Yan et al., 2009; Hayashida et al., 2013) while the persistent deep convection results the updraft of CH₄-laden air mass from surface to the upper troposphere during the same season, where CH₄ is further spread over larger region by the anticyclonic winds (Patra et al., 2011b; Baker et al., 2012; Schuck et al., 2012). Several studies highlighted the role of convective transport of pollutants (including CH₄) from surface to the upper troposphere (400 – 200 hPa) during SW monsoon season (July-September) (Park et al., 2004; Randel et al., 2006; Xiong et al., 2009; Patra et al., 2011b; Baker et al., 2012; Schuck et al., 2012; Lal et al., 2014; Chandra et al., 2016). The dynamical system dominated by deep convection and anticyclone cover mostly the northern Indian region (north of 15°N) due to the presence of the Himalayas and the Tibetan Plateau, while such complex dynamical system has not been observed over the southern part of India (south of 15°N) (Rao, 1976).

Satellite-based measurements show elevated levels of XCH₄ over the northern part of India (north of 15°N) particularly high over IGP during the SW monsoon season (July to September) and over southern India (south of 15°N) during early autumn season (October to December) (Frankenberg et al., 2008, 2011; Hayashida et al., 2013). Previous studies have linked these high XCH₄ levels to the strong surface CH₄ emissions particularly from the rice cultivation over the Indian region, because they showed statistically significant correlations over certain regions (Hayashida et al., 2013; Kavitha et al., 2016). The differences in the peak of XCH₄ seasonal cycle over northern and southern regions of India are discussed on the basis of agricultural practice in India that takes place in two seasons, May to October and November to April, respectively. However, inferring local emissions directly from variations in XCH₄ is ambiguous particularly over the Indian regions under the influence of monsoon meteorology, because XCH₄ involves contributions of CH₄ abundances from all altitudes along the solar light path. Though, vertically resolving retrieval products of CH₄ are available from the Thermal InfraRed (TIR) channel of GOSAT, but these products are still under validation (e.g., Zou et al., 2016, Olsen et al., 2017). The other infrared sensors such as Atmospheric Infrared Sounder (AIRS), Tropospheric Emission Spectrometer (TES) and Infrared Atmospheric Sounding Interferometer (IASI) are not sufficiently sensitive to the lower troposphere (e.g., Worden et al., 2015).

This study attempts for the first time to separate the factors responsible (emission, transport and chemistry) for the distributions of columnar methane (XCH₄) over the Asian monsoon region for different altitude segments. The XCH₄ mixing ratios are used for this study as observed from GOSAT and simulated by JAMSTEC's ACTM. We aim to understand relative contributions of surface emissions and transport in formation of XCH₄ seasonal cycles over different parts of India and the surrounding oceans. This understanding will help us towards making an inverse modelling system for estimation of CH₄ surface emissions using XCH₄ observations and ACTM forward simulation.

2. Methods

2.1 Satellite data:

The Greenhouse gases Observing SATellite (GOSAT) (also referred to as Ibuki) is a joint satellite project of the National Institute of Environmental Studies (NIES), Ministry of the Environment (MOE) and Japan Aerospace Exploration Agency (JAXA). It has been providing columnar dry air mole fractions of the two important greenhouse gases (XCH₄ and XCO₂) at near global coverage since its launch in January 2009. It is equipped onboard with the Thermal And Near infrared Sensor for carbon Observation-Fourier Transform Spectrometer (TANSO-FTS) and the Cloud and Aerosol Imager (TANSO-CAI) (Kuze et al., 2009). To avoid cloud contamination in the retrieval process, any scene with more than one cloudy pixel within the TANSO-FTS IFOV is excluded. The atmospheric images from CAI are used to identify the cloudy pixels. As a result of this strict screening, only limited numbers of XCH₄ data are available during the SW monsoon over South Asia. This study uses the GOSAT SWIR XCH₄ (Version 2.21)-Research Announcement product for the period of 2011-2014. The ground-based FTS measurements of XCH₄ by the Total Carbon Column Observing Network (TCCON) (Wunch et al., 2011) are used extensively to validate the GOSAT retrievals. Retrieval bias and precision of column abundance from GOSAT SWIR observations have been estimated as approximately 15-20 ppb and 1%, respectively for the NIES product using TCCON data (Morino et al., 2011; Yoshida et al., 2013).

2.2. Model simulations

Model analysis is comprised of simulations from the JAMSTEC's atmospheric general circulation model (AGCM)-based chemistry-transport model (ACTM; Patra et al., 2009). The AGCM was developed by the Center for Climate System Research/National Institute for Environmental Studies/Frontier Research Center for Global Change (CCSR/NIES/FRCGC). It has been a part of the transport model inter-comparison experiment TransCom-CH₄ (Patra et al., 2011a) and used in inverse modeling of CH₄ emissions (Patra et al., 2016). The ACTM runs at a horizontal resolution of T42 spectral truncations ($\sim 2.8^\circ \times 2.8^\circ$) with 67 sigma-pressure vertical levels. The evolution of CH₄ at different longitude (x), latitude (y) and altitude (z) with time in the Earth's atmosphere depends on the surface emission, chemical loss and transport, which can be mathematically represented by the following continuity equation:

$$\frac{dCH_4(x, y, z, t)}{dt} = S_{CH_4}(x, y, t) - L_{CH_4}(x, y, z, t) - \nabla \cdot \phi(x, y, z, t)$$

where

CH₄ = methane molar fraction in the atmosphere

S_{CH₄} = Total emissions/sinks of CH₄ at the surface

L_{CH₄} = Total loss of CH₄ in the atmosphere due to the chemical reactions

$\nabla \cdot \phi$ = Transport of CH₄ due to the advection, convection and diffusion.

The meteorological fields of ACTM are nudged with reanalysis data from the Japan Meteorological Agency, version JRA-25 (Onogi et al., 2007). The model uses an optimal OH field (Patra et al., 2014) based on a scaled version of the seasonally varying OH field (Spivakovsky et al., 2000). The a priori anthropogenic emissions are from Emission Database for Global Atmospheric Research (EDGAR) v4.2 FT2010 database (<http://edgar.jrc.ec.europa.eu>). The model sensitivity for emission is examined by two cases of emission scenarios based on different combination of sectorial emissions. First one is referred by the AGS, where all emission sectors in EDGAR42FT are kept at a constant value for 2000, except for emissions from agriculture soils. The second one is controlled emission scenario referred by CTL, which is based on the ensemble of the anthropogenic emissions from EDGAR32FT (as in Patra et al., 2011a), wetland and biomass burning emissions from Fung et al. (1991) and rice paddies emission from Yan et al. (2009). The emission seasonality differs substantially between the CTL case and the AGS case due to differences in emissions from wetlands, rice paddies and biomass burning; other anthropogenic emissions do not contain seasonal variations (Patra et al., 2016). Further details about the model and these emission scenarios can be found in the previous studies (Patra et al., 2009; Patra et al., 2011a; Patra et al., 2016).

XCH₄ is calculated from the ACTM profile using following equations:

$$XCH_4 = \sum_{n=1}^{60} CH_4(n) \times \Delta\sigma_p(n)$$

where, CH₄(n) is the dry-air mole fraction at model mid-point level, n = number of vertical sigma pressure layers of ACTM (= 1-60 with σ_p values of 1.0 and 0.005), $\Delta\sigma_p$ = thickness of sigma pressure level. Note here that we have not incorporated convolution of model profiles with retrieval a priori and averaging kernels. Because the averaging kernels are nearly constant in the troposphere (Yoshida et al., 2011), hence this approximation does not lead to serious errors in constructing the model XCH₄. The seasonal distributions of partial columnar CH₄ (denoted by X_pCH₄) for a thickness of 0.2 sigma pressure layers are used to understand the contribution of different layers to the total XCH₄ seasonal cycle. For both the CTL and AGS cases, we adjust a constant offset of 20 ppb to the modeled time series, which should make the *a priori* correction have a lesser impact on the

model XCH₄. Because the focus of this study is seasonal and spatial variations in XCH₄, a constant offset adjustment should not affect the main conclusions. XCH₄ data are sampled at the nearest model grid from the available observations and satellite overpass time (~ 1300 hrs LT) and then averaged over the selected partitions of the study region (Figure 2a).

3. Results and discussion

3.1 XCH₄ over the Indian region: View from GOSAT and ACTM simulations

This section presents an analysis of XCH₄ observed by GOSAT from Jan 2011 to Dec 2014 over the Indian region. We characterize the 4 seasons specific to the region as winter (January to March), spring (April to June), summer (July to September) or the SW monsoon, and autumn (October to December). Since general features of XCH₄ simulated by ACTM using emission scenarios AGS and CTL are similar to each other, the main discussion is made using AGS scenario only. Figure 1a-b show that the XCH₄ mixing ratios are lower during the spring season and higher during the autumn season. A strong latitudinal gradient in XCH₄ is observed between the Indo-Gangetic Plain (IGP) and the other parts of India. XCH₄ show the highest value (~1880 ppb) over the IGP, eastern and northeast Indian regions. As seen from Figure 1c-d, ACTM simulations are able to reproduce the observed latitudinal and seasonal gradients in XCH₄; i.e., higher values during the southwest monsoon and autumn seasons and lower values during the winter and spring seasons over the IGP region. The optimized total CH₄ fluxes (AGS and CTL) show high emissions over the IGP region and northeast Indian regions (Figure 1e-f). Most elevated levels of XCH₄ are often observed simultaneously with the higher emissions, suggesting a link between the enhanced XCH₄ and high surface emissions in the summer season. However, this connection is not valid over all locations. For example, over western and southern region of India, XCH₄ is higher in autumn than in spring, though the emissions are higher in spring.

To study the seasonal XCH₄ pattern in details depending on the distinct spatial pattern of surface emissions and XCH₄ mixing ratios shown in Figure 1, the Indian landmass was partitioned into eight sub-regions: Northeast India (NEI), Eastern India (EI), Eastern IGP (EIGP), Western IGP (WIGP), Central India (CI), Arid India (AI), Western India (WI), Southern Peninsula (SP), and two surrounding oceanic regions, the Arabian Sea (AS) and Bay of Bengal (BOB) (Figure 2a). Regional divisions are made based on spatial patterns of emission and XCH₄ (Figure 1a-f), and our knowledge of seasonal meteorological conditions. Figure 2b-k shows ACTM - GOSAT comparisons of XCH₄ time series from Jan 2011 to Dec 2014 over the selected study regions. The climatological means resulting from the time series shown in Figure 2 is provided in the supplementary information (Figure S1). Observations are limited during the SW monsoon season due to GOSAT retrieval limitations under cloud cover. The model captures the salient features in the seasonal cycles at very high statistical significance as indicated by the high correlation coefficients ($r > 0.6$) over the selected regions (refer to supplementary Table S1). As shown in Table S1, the highest correlation coefficients between the GOSAT measurements and ACTM simulations are obtained over SP region and also over oceanic regions (AS and BOB). The high ACTM-GOSAT correlations for the low/no emission regions suggest that transport and chemistry are accurately modeled in ACTM. Although we do not have statistically significant number of observations for the SW monsoon period, the GOSAT data showing high XCH₄ during this period were generally well simulated by ACTM over most of the study regions. Based on these comparisons, we can assume that model simulations can be used to understand XCH₄ variability over the Indian region. Though we showed only the pairs of data of GOSAT and ACTM that matched in time and location in Figure 2, we also confirmed that the correlation is high ($r \sim 0.9$) between the averaged time series over different regions with and without sampling of model at the location and time of GOSAT sampling. This high correlation assures representativeness of the data shown in Figure 2. Thus, the seasonal evolution of XCH₄ using the ACTM simulations alone is

expected to be fairly valid for different altitude layers (ref. to Patra et al., 2011b for comparison at the aircraft cruising altitude). Though the model is only validated for XCH₄ in this study, comparisons with surface and aircraft CH₄ observations have been shown in Patra et al. (2016).

3.2 Seasonal cycle of XCH₄ and possible controlling factors

As mentioned earlier, that the persistent deep convection and mean circulation during the SW monsoon season significantly enhance CH₄ in the upper troposphere (e.g., Xiong et al., 2009, Baker et al., 2012), coinciding with the period of high surface CH₄ emissions due to rice paddy cultivation and wetlands over the Indian region (Yan et al., 2009; Hayashida et al., 2013). Both these emission and transport processes contribute greatly to seasonal changes in XCH₄, although their relative contributions have not been studied over the monsoon dominated Indian region. For understanding the role of transport, the atmospheric column is segregated into five sigma-pressure (σ_p) layers, starting from the surface level ($\sigma_p = 1$) to top of the atmosphere ($\sigma_p = 0$) with an equal spacing of 0.2. The layers bounded by the boundaries between 1.0-0.8, 0.8-0.6, 0.6-0.4, 0.4-0.2, and 0.2-0.0 of sigma pressure are denoted by LT, MT1, MT2, UT and UA, respectively. The partial columnar CH₄ are calculated within different σ_p layers (denoted by X_pCH₄) using the same formula for XCH₄, as in Section 2.2. The model results are averaged over each sub-region of our analysis for XCH₄ seasonal cycle. For understanding the role of surface emission in formation of XCH₄ seasonal cycle, the climatology of optimized total CH₄ flux for each sub-region are used. Figure 3 shows the climatology (2011-2014) of total CH₄ flux, XCH₄ and X_pCH₄ from the model averaged over three selected regions, EIGP, SP and AI. The observed GOSAT XCH₄ values are also shown for comparison. However note that this comparison is just for a reference because the model results are not collocated with sampling location and time of GOSAT, which is different from the case in Fig. 2. These representative regions have been selected because they show distinct XCH₄ seasonal cycles and the dominant controlling factors (such as emission, transport and chemistry). The figures for the remaining seven regions are available in the supplementary information (Figures S2, S3).

Over the EIGP region, magnitude and timing of seasonal peak in emission differ substantially between the CTL and AGS emission scenarios (ref. Figure 3g). ACTM simulated XCH₄ seasonal peak is in agreement with peak in emission in June for AGS case and in August for CTL case (Figure 3f). However, simulated XCH₄ remains nearly constant until September, although the emission decreases substantially toward winter. In general, emission is relatively higher in monsoon season (July-August-September) than in other seasons in both cases. However, in the LT, where we expect most susceptible to the surface emission, the partial column CH₄ indicates very different seasonality from the emissions; X_pCH₄ (LT) increases toward winter continuously (Figure 3e). The partial CH₄ columns for the upper troposphere and middle troposphere (Figure 3b-c) show similar seasonality to the total XCH₄ rather than in the LT. Therefore, this analysis strongly suggest that both the emissions on Earth's surface and the upper tropospheric partial column contribute to the formation of XCH₄ seasonal cycle. These results also suggest the possibility that GOSAT and ACTM XCH₄ data can be used for correcting a priori emission scenarios by inverse modelling.

In contrast to the XCH₄ seasonal cycle over EIGP, a notable difference is observed in the emission and XCH₄ seasonal cycle over the SP region (Fig. 2h-n). The XCH₄ seasonal cycle and emission seasonal cycle are found to be out of phase with each other and the differences in emission scenarios are not reflected in XCH₄ seasonal variations. Both emission scenarios show distinct seasonal pattern; AGS shows annual high emissions from April to September, while CTL shows annual high during August-September (Figure 3n). It should be noted that the total emissions are much lower than that of EIGP (note the different y-axis

scale of emissions in Figure 3n) and hence the difference between the XCH_4 simulations from both emission scenarios is comparatively low. The XCH_4 shows almost identical seasonal cycles for both of the emission scenarios, a peak in October and prolonged low values during May to September. The seasonal X_pCH_4 cycle in the LT layer shows seasonal pattern similar to the total XCH_4 . Inconsistency between emission seasonality and XCH_4 coupled with low emissions strongly suggests that the XCH_4 can be controlled by transport and/or chemistry, but not emissions. Surface winds from May to September over SP are from the southern hemisphere, which effectively flushes the air with low CH_4 and pushes the polluted air masses from the south to the north India region (ref. Figure S4). Further, the distinct seasonal cycle of chemical loss is observed over the SP region (ref. Figure S5) compared to other study regions; the loss rate starts increasing from 6 ppb day⁻¹ in January to 12 ppb day⁻¹ in April, reaching a plateau from April to September (~12 ppb day⁻¹). These evidences clearly suggest that the combined effect of transport and chemistry causes the low XCH_4 values for the May-September period over the SP region. The peaks in the upper layers (Figure 3k-h) in October and transport from polluted continental layer in the LT layer (ref. Figure S4) could together contribute to the seasonal XCH_4 peak over SP. As shown here clearly that the XCH_4 measurements do not allow us derive a strong constraint on surface emissions in the inverse analysis over the southern India region, suggesting a need for in situ measurements.

Over the Arid Indian (AI) region, XCH_4 seasonal cycle is observed to be different from those of the EIGP and SI regions. The simulated XCH_4 (Figure 3t) show extremely weak sensitivity to the surface emission differences between the AGS and CTL cases (Figure 3u). Additionally, the X_pCH_4 in the LT layer (Figure 3s), which must follow the surface emission, does not resemble with the phase of seasonal surface emissions and simulated XCH_4 . The X_pCH_4 in the LT layer decreases from Jan to August and increases until December. On the other hand, in XCH_4 , a remarkable peak (~1896 ppb) is observed in August followed a decline afterward (Figure 3t). This is an outstanding example of deceiving linkage between surface emissions and XCH_4 in terms of seasonal variation. An enhancement in the mixing ratios of X_pCH_4 is observed from May to August only in the MT2 and UT layers (Figure 3p-q) and from June to August in the UA layer (Figure 3o). This analysis infers that MT2 and UT partial columns mostly contribute in the formation of XCH_4 seasonal cycle over AI region.

Next, we quantify the contributions of different partial layers (X_pCH_4) in formation of XCH_4 seasonal amplitude. We calculate the differences of the X_pCH_4 values at the time of peak and trough of the XCH_4 seasonal cycle over each region taken from ACTM simulations (Figure 4). Note that the phase of X_pCH_4 seasonal variation do not match always with that of XCH_4 , thus the fixed timing of peak and trough in XCH_4 is used for all of the X_pCH_4 time series. Further, these differences at different partial layers are divided by seasonal amplitude of XCH_4 and then multiplied by 100 for calculating the percentage contributions from respective layers into the seasonal amplitude of XCH_4 . These results reveal that ~40% of the seasonal enhancement in the observed XCH_4 can be attributed to the partial pressure layers below 600 hPa (LT and MT1) for EIGP region, which are directly influenced by the surface emissions (Figure 4). About 40% in seasonal enhancement comes from layers above 600 hPa. Over the SP region, about 60% of the seasonal XCH_4 amplitude is attributed to layers below 600 hPa and remaining 40% results from the upper layers. Although the activities in the lower atmosphere (below 600 hPa) govern most of the seasonal XCH_4 cycle over this region, there is not clear link with seasonal variations in emissions as this region is under greater influence of changes in monsoon meteorology. These regions are under the influence of emission signals from the Indian subcontinent during winter; while in the summer, clean marine air control CH_4 levels (see also Patra et al., 2009). In contrast to the two regions mentioned above, over the AI region, the LT and MT1 layers together contribute only about 12% to the formation of XCH_4 seasonal cycle

amplitude, and the layers above 600 hPa contribute to the remaining 88%. These findings lead us to conclude that instead of surface emissions, the high CH_4 in the upper tropospheric layers contribute significantly to the formation of seasonal peaks in XCH_4 .

3.3 Source of higher CH_4 in the upper troposphere

Using ACTM simulations, we have shown that the higher CH_4 levels in the upper tropospheric region ($\sim 400\text{--}200$ hPa) during the monsoon season contribute significantly to enhanced XCH_4 values over northern India regions. The reason of high mixing ratios in the upper troposphere, as discussed in the former section, can be explained by vertical transport of the CH_4 from the surface, because the vertical transport timescales in the tropical region is much shorter than chemical lifetime of CH_4 of the order of 1-2 years (Patra et al., 2009). Figure 5a-d shows the latitudinal cross section of the convective transport rate (in ppb day^{-1}) along with height and vertical velocity (hPa s^{-1}) averaged over $83\text{--}93^\circ\text{E}$ for different seasons in 2011 (the ACTM AGS case). The positive/negative values of convective transport rate and vertical velocity in Figure 5a-d indicate the gain/loss of mass and downward/upward motions, respectively. Rapid updrafts of CH_4 , as indicated by higher negative values of vertical velocity, by deep convection during the monsoon season are aided by the local topography over the IGP region (north of 20°N and east of 79°E in the Indian region). These updrafts lift CH_4 -rich air into the upper tropospheric region (Figure 5g). The CH_4 concentrations at the surface level decrease by dissipation at an average rate of $\sim 10 \text{ ppb day}^{-1}$ during Spring-Autumn seasons (Figure 5b-d), and accumulate in the upper troposphere at a similar rate; the height of peak accumulation varies with season.

The horizontal map of CH_4 at 200 hPa is shown with wind vectors in Figure 5i-l for understanding the spatial extent of uplifted CH_4 -rich air over the whole South Asian region. The CH_4 -rich air mass in the upper troposphere (~ 200 hPa) is then encountered by the anticyclonic winds during the SW monsoon season, which trap CH_4 and lead to widespread CH_4 enhancement covering large part of South Asia, and the CH_4 enhancement extends through the East Asia (Figure 5k). As a result of this, the high CH_4 air masses at upper troposphere, are not limited over the regions of intense surface emissions as discussed earlier. After the SW monsoon season, the high westerly jet breaks the upper tropospheric anticyclone and the CH_4 -rich air mass shifts over southern India during the autumn season (Figure 5l). In this way, the convective updraft of high- CH_4 air mass, followed by horizontal spreading of the air mass over the larger area by anticyclonic circulation, controls redistribution of CH_4 in the upper troposphere over the northern part of India during SW monsoon season, and over southern peninsula during the early autumn season.

4. Conclusions

The dry-air mole fractions of methane (XCH_4) measured by GHGs Observation SATellite (GOSAT) are analyzed over India and the surrounding seas using the JAMSTEC's atmospheric chemistry-transport model (ACTM). The region of interest (Indian landmass) is divided into 8 sub-regions, namely, Northeast India (NEI), Eastern India (EI), Eastern IGP (EIGP), Western IGP (WIGP), Central India (CI), Arid India (AI), Western India (WI), Southern Peninsula (SP), and two surrounding oceanic regions, the Arabian Sea (AS) and Bay of Bengal (BOB). The ACTM simulations are conducted using a couple of surface fluxes optimized by the inverse analysis as described in Patra et al. (2013). We have shown that the distinct spatial and temporal variations of XCH_4 observed by GOSAT are not only governed by the heterogeneity in surface emissions, but also due to complex atmospheric transport mechanisms caused by the seasonally varying Asian monsoon. The seasonal XCH_4 patterns often show a fair correlation between emissions and XCH_4 over the regions residing in the northern half of India (north of 15°N : NEI,

EI, EIGP, WIGP, CI, WI, AI), which would imply XCH₄ levels are closely associated with the distribution of emissions on the Earth's surface. However, detailed analysis of transport and emission using ACTM over these regions (except for the AI) reveal that about 40% of seasonal enhancement in the observed XCH₄ can be attributed to the lower tropospheric layer (below 600 hPa). The lower tropospheric layer are either affected by the surface emissions, e.g., in the northern India regions or seasonal changes in horizontal winds due to monsoon for the SP, AS and BoB regions. Up to 40% of the seasonal CH₄ enhancement is found to come from the uplifted air mass in to the 600-200 hPa height layer over northern regions in India. In contrast, over semi-arid AI region, as much as ~88% contributions to the XCH₄ seasonal cycle amplitude come from the height above 600 hPa, and only ~12% are contributed by the atmosphere below 600 hPa. The primary cause of the higher contributions from above 600 hPa over the northern Indian region is the characteristic air mass transport mechanisms in the Asian monsoon region. The persistent deep convection during the southwest monsoon season (June-August) causes strong updrafts of CH₄ from the surface to upper troposphere, which is then distributed by anticyclonic winds over wider area of the northern India. These transport mechanisms caused the elevated CH₄ mixing ratios in the upper troposphere hence contributed significantly to the seasonal peak in XCH₄ over northern India. In contrast to these regions, over the SP region, the major contributions (about 60%) to XCH₄ seasonal amplitude come from the lower atmosphere (~1000-600 hPa). Both transport and chemistry dominate in the lower troposphere over SP region and thus the formation of XCH₄ seasonal cycle is not consistent with the seasonal cycle of local emissions. As the upper level anticyclone does not cover the southern Indian region in the active phase of southwest monsoon, no enhancement in XCH₄ is observed over the southern peninsular region.

This study shows that ACTM simulations are generally capturing the GOSAT observed seasonal and spatial XCH₄ variability and points to a comprehensive understanding of emissions, chemistry and transport of CH₄ over one of the strongest global monsoonal regions is extremely important for perceptive insights into the source-receptor relationships. Our results provide strong support for performing inverse modelling of CH₄ surface emissions in the future using XCH₄ observations and ACTM forward simulation.

Acknowledgements

The Environment Research and Technology Development Fund (A2-1502) of the Ministry of the Environment, Japan, supported this research. The data used for preparing the figures, and table could be available on request. The corresponding author may be contacted for the same.

References

- Baker, A. K., Schuck, T. J., Brenninkmeijer, C. A. M., Rauthe-Schöch, A., Slemr, F., van Velthoven, P. F. J., and Lelieveld, J.: Estimating the contribution of monsoon-related biogenic production to methane emissions from South Asia using CARIBIC observations, *Geophys. Res. Lett.*, 39, L10813, doi:10.1029/2012GL051756, 2012.
- Crutzen, P.J., Aselmann, I., and Seiler, W.: Methane production by domestic animals, wild ruminants other herbivorous fauna and humans. *Tellus* 38B, 271-284, doi:10.1111/j.1600-0889.1986.tb00193.x, 1986.
- Cao, M., Gregson, K., and Marshall, S.: Global methane emission from wetlands and its sensitivity to climate change. *Atmos. Environ.* 32 (19), 3293-3299, doi:10.1016/S1352-2310 (98) 00105-8, 1998.

- Chandra, N., Venkataramani, S., Lal, S., Sheel, V. & Pozzer, A.: Effects of convection and long-range transport on the distribution of carbon monoxide in the troposphere over India. *Atmospheric Pollution Research* 7, 775 – 785, doi:10.1016/j.apr.2016.03.005, 2016.
- Dlugokencky, E. J., Nisbet, E. G., Fisher, R., and Lowry, D.: Global atmospheric methane: Budget, changes, and dangers, *Philos. Trans. R. Soc. London, Ser. A.*, 369, 2058–2072, 2011.
- EDGAR42FT, 2013: Global emissions EDGAR v4.2FT2010 (October 2013). [Available at <http://edgar.jrc.ec.europa.eu/overview.php?v=42FT2010>.]
- Fung, I., John, J., Lerner, J., Matthews, E., Prather, M., Steele, L. P., and Fraser, P. J.: Three-dimensional model synthesis of the global methane cycle, *J. Geophys. Res.*, 96, 13033–13065, doi:10.1029/91JD01247, 1991
- Frankenberg, C., P. Bergamaschi, A. Butz, S. Houweling, J. F. Meirink, J. Notholt, A. K. Petersen, H. Schrijver, T. Warneke, and I. Aben (2008), Tropical methane emissions: A revised view from SCIAMACHY onboard ENVISAT, *Geophys. Res. Lett.*, 35(15), doi:10.1029/2008gl034300.
- Frankenberg, C., I. Aben, P. Bergamaschi, E. J. Dlugokencky, R. van Hees, S. Houweling, P. van der Meer, R. Snel, and P. Tol (2011), Global column-averaged methane mixing ratios from 2003 to 2009 as derived from SCIAMACHY: Trends and variability, *J. Geophys. Res.*, 116(D4), doi:10.1029/2010jd014849.
- Hayashida, S., Ono, A., Yoshizaki, S., Frankenberg, C., Takeuchi, W., Yan, X.: Methane concentrations over Monsoon Asia as observed by SCIAMACHY: Signals of methane emission from rice cultivation. *Remote Sensing of Environment* 139, 246–256, doi: 10.1016/j.rse.2013.08.008, 2013.
- Kuze, A., Suto, H., Nakajima, M., and Hamazaki, T.: Thermal and near infrared sensor for carbon observation Fourier transform spectrometer on the Greenhouse Gases Observing Satellite for greenhouse gases monitoring. *Appl. Opt.* 48, 6716–6733, doi: 10.1364/AO.48.006716, 2009.
- Kar, J., Deeter, M. N., Fishman, J., Liu, Z., Omar, A., Creilson, J. K., Trepte, C. R., Vaughan, M. A., and Winker, D. M.: Wintertime pollution over the Eastern Indo-Gangetic Plains as observed from MOPITT, CALIPSO and tropospheric ozone residual data, *Atmos. Chem. Phys.*, 10, 12273–12283, doi:10.5194/acp-10-12273-2010, 2010.
- Kavitha, M. and Nair, P. R.: Region-dependent seasonal pattern of methane over Indian region as observed by SCIAMACHY. *Atmospheric Environment* 131, 316–325, doi:10.1016/j.atmosenv.2016.02.008, 2016.
- Lal, S., Venkataramani, S., Chandra, N., Cooper, O. R., Brioude, J., and Naja, M.: Transport effects on the vertical distribution of tropospheric ozone over western India, *J. Geophys. Res. Atmos.*, 119, 10,012–10,026, doi:10.1002/2014JD021854, 2014.
- Matthews, E., and Fung, I.: Methane emissions from natural wetlands: Global distribution, area and environmental characteristics of sources. *Global Biogeochem. Cycles* 1, 61–86, 1987.
- Minami, K., and Neue, H. U.: Rice paddies as a methane source. *Clim. Change Lett.* 27, 13–26, doi:10.1007/BF01098470, 1994.
- Morino, I., Uchino, O., Inoue, M., Yoshida, Y., Yokota, T., Wennberg, P. O., Toon, G. C., Wunch, D., Roehl, C. M., Notholt, J., Warneke, T., Messerschmidt, J., Griffith, D. W. T., Deutscher, N. M., Sherlock, V., Connor, B., Robinson, J., Sussmann, R., and Rettinger, M.: Preliminary validation of column-average volume mixing ratios of carbon dioxide and methane retrieved from GOSAT short-wavelength infrared spectra. *Atmos. Meas. Tech.*, 4, 1061–1076, doi:10.5194/amt-4-1061-2011, 2011.
- Myhre, G., Shindell, D., Bréon, F.-M., Collins, W. Fuglestad, J., Huang, J., Koch, D. Lamarque, J.-F., Lee, D., Mendoza, B., Nakajima, T., Robock, A., Stephens, G. Takemura, T., and Zhang, H.: Anthropogenic and natural radiative forcing, in: *Climate Change 2013: The Physical Science Basis, Fifth Assessment Report of the Intergovernmental Panel on Climate Change*, edited by: Stocker, T. F. et al., Cambridge University Press, Cambridge, UK, New York, NY, USA, 659–740, 2013.

- Olivier, J. G. J., Aardenne, J.A.V., Dentener, F., Ganzeveld, L. N., Peters, J.A.H.W.: Recent trends in global greenhouse gas emissions: Regional trends and spatial distribution of key sources, in: *Non-CO₂ Greenhouse Gases (NCGG-4)*, edited by: van Amstel, A., 325–330, Millpress, Rotterdam, Netherlands, 2005.
- Onogi, K., Tsutsui, J., Koide, H., Sakamoto, M., Kobayashi, S., Hatsushika, H., Matsumoto, T., Yamazaki, N., Kamahori, H., Takahashi, K., Kadokura, S., Wada, K., Kato, K., Oyama, R., Ose, T., Mannoji, N., and Taira, R.: The JRA-25 reanalysis, *J. Meteorol. Soc. Jpn.*, 85, 369–432, 2007.
- Olsen, K. S., Strong, K., Walker, K. A., Boone, C. D., Raspollini, P., Plieninger, J., Bader, W., Conway, S., Grutter, M., Hannigan, J. W., Hase, F., Jones, N., de Mazière, M., Notholt, J., Schneider, M., Smale, D., Sussmann, R., and Saitoh, N.: Comparison of the GOSAT TANSO-FTS TIR CH₄ volume mixing ratio vertical profiles with those measured by ACE-FTS, ESA MIPAS, IMK-IAA MIPAS, and 16 NDACC stations, *Atmos. Meas. Tech. Discuss.*, doi:10.5194/amt-2017-6, in review, 2017.
- Park, M., Randel, W. J., Kinnison, D. E., Garcia, R. R., and Choi, W.: Seasonal variation of methane, water vapor, and nitrogen oxides near the tropopause: Satellite observations and model simulations. *Journal of Geophysical Research: Atmospheres* 109, doi: 10.1029/2003JD003706. D03302, 2004.
- Patra, P. K., Takigawa, M., Ishijima, K., Choi, B. C., Cunnold, D., Dlugokencky, E. J., Fraser, P., A. J., Gomez-Pelaez, Goo, T. Y., Kim, J. S., Krummel, P., Langenfelds, R., Meinhardt, F., Mukai, H., O'Doherty, S., Prinn, R. G., Simmonds, P., Steele, P., Tohjima, Y., Tsuboi, K., Uhse, K., Weiss, R., Worthy, D., and Nakazawa, T.: Growth rate, seasonal, synoptic, diurnal variations and budget of methane in lower atmosphere, *J. Meteorol. Soc. Jpn.*, 87(4), 635–663, doi: 10.2151/jmsj.87.635, 2009.
- Patra, P. K., Houweling, S., Krol, M., Bousquet, P., Belikov, D., Bergmann, D., Bian, H., Cameron-Smith, P., Chipperfield, M. P., Corbin, K., Fortems-Cheiney, A., Fraser, A., Gloor, E., Hess, P., Ito, A., Kawa, S. R., Law, R. M., Loh, Z., Maksyutov, S., Meng, L., Palmer, P. I., Prinn, R. G., Rigby, M., Saito, R., and Wilson, C.: TransCom model simulations of CH₄ and related species: Linking transport, surface flux and chemical loss with CH₄ variability in the troposphere and lower stratosphere, *Atmos. Chem. Phys.*, 11, 12,813–12,837, doi:10.5194/acp-11-12813-2011, 2011a.
- Patra, P. K., Niwa, Y., Schuck, T. J., Brenninkmeijer, C. A. M., Machida, T., Matsueda, H., and Sawa, Y.: Carbon balance of South Asia constrained by passenger aircraft CO₂ measurements, *Atmos. Chem. Phys.*, 11, 4163–4175, doi:10.5194/acp-11-4163-2011, 2011b.
- Patra, P. K., Canadell, J. G., Houghton, R. A., Piao, S. L., Oh, N.-H., Ciais, P., Manjunath, K. R., Chhabra, A., Wang, T., Bhattacharya, T., Bousquet, P., Hartman, J., Ito, A., Mayorga, E., Niwa, Y., Raymond, P. A., Sarma, V. V. S. S., and Lasco, R.: The carbon budget of South Asia, *Biogeosciences*, 10, 513–527, doi:10.5194/bg-10-513-2013, 2013.
- Patra, P. K., Krol, M. C., Montzka, S. A., Arnold, T., Atlas, E. L., Lintner, B. R., Stephens, B. B., Xiang, B., Elkins, J. W., Fraser, P. J., Ghosh, A., Hintsa, E. J., Hurst, D. F., Ishijima, K., Krummel, P. B., Miller, B. R., Miyazaki, K., Moore, F. L., Mühle, J., O'Doherty, S., Prinn, R. G., Steele, L. P., Takigawa, M., Wang, H. J., Weiss, R. F., Wofsy, S. C., and Young, D.: Observational evidence for interhemispheric hydroxyl parity, *Nature*, 513, 219–223, 2014.
- Patra, P. K., Saeki, T., Dlugokencky, E. J., Ishijima, K., Umezawa, S. T., Ito, A., Aoki, S., Morimoto, S., Kort, E. A., Crotwell, A., Kumar, R., and Nakazawa, T.: Regional methane emission estimation based on observed atmospheric concentrations (2002–2012), *J. Meteorol. Soc. Jpn.*, 94(1), 91–113, doi:10.2151/jmsj.2016-006, 2016.
- Rao, Y. P.: Southwest monsoon: Synoptic Meteorology, *Meteor. Monogr.*, No. 1/1976, India Meteorological Department, 367 pp, 1976.

- Randel, W. J. and Park, M.: Deep convective influence on the Asian summer monsoon anticyclone and associated tracer variability observed with Atmospheric Infrared Sounder (AIRS). *J. Geophys. Res.* 111, doi: 10.1029/2005JD006490, 2006.
- Sugimoto, A., Inoue, T., Kirtibutr, N. and Abe, T.: Methane oxidation by termite mounds estimated by the carbon isotopic composition of methane. *Glob. Biogeochem. Cycles* 12 (4), 595-605, doi:10.1029/98GB02266, 1998.
- Shindell, D. T., Faluvegi, G., Koch, D. M., Schmidt, G. A., Unger, N., Bauer, S. E.: Improved attribution of climate forcing to emissions, *Science*, 326, 716-718, doi: 10.1126/science.1174760, 2009.
- Schuck, T. J., Ishijima, K., Patra, P. K., Baker, A. K., Machida, T., Matsueda, H., Sawa, Y., Umezawa, T., Brenninkmeijer, C. A. M., and Lelieveld, J.: Distribution of methane in the tropical upper troposphere measured by CARIBIC and CONTRAIL aircraft, *J. Geophys. Res.*, 117, D19304, doi:10.1029/2012JD018199, 2012.
- Spivakovsky, C. M., Logan, J. A., Montzka, S. A., Balkanski, Y. J., Foreman-Fowler, M., Jones, D. B. A., Horowitz, L. W., Fusco, A. C., Brenninkmeijer, C. A. M., Prather, M. J., Wofsy, S. C., and McElroy, M. B.: Three-dimensional climatological distribution of tropospheric OH: update and evaluation, *J. Geophys. Res.*, 105, 8931-8980, doi:10.1029/1999JD901006, 2000.
- Worden, J. R., Turner, A. J., Bloom, A., Kulawik, S. S., Liu, J., Lee, M., Weidner, R., Bowman, K., Frankenberg, C., Parker, R., and Payne, V. H.: Quantifying lower tropospheric methane concentrations using GOSAT near-IR and TES thermal IR measurements, *Atmos. Meas. Tech.*, 8, 3433-3445, doi:10.5194/amt-8-3433-2015, 2015.
- Wunch, D., G. C. Toon, J.-F. L. Blavier, R. A. Washenfelder, J. Notholt, B. J. Connor, D. W. T. Griffith, V. Sherlock, and P. O. Wennberg, The total carbon column observing network, *Phil. Trans. Royal Society - Series A*, 369, 2087-2112, doi:10.1098/rsta.2010.0240, 2011.
- Xiong, X., Houweling, S., Wei, J., Maddy, E., Sun, F., and Barnet, C.: Methane plume over south Asia during the monsoon season: satellite observation and model simulation, *Atmos. Chem. Phys.*, 9, 783-794, doi:10.5194/acp-9-783-2009, 2009.
- Yoshida, Y., Y. Ota, N. Eguchi, N. Kikuchi, K. Nobuta, H. Tran, I. Morino, and T. Yokota (2011), Retrieval algorithm for CO₂ and CH₄ column abundances from short-wavelength infrared spectral observations by the Greenhouse gases observing satellite, *Atmospheric Measurement Techniques*, 4(4), 717-734, doi:10.5194/amt-4-717-2011.
- Yoshida, Y., Kikuchi, N., Morino, I., Uchino, O., Oshchepkov, S., Bril, A., Saeki, T., Schutgens, N., Toon, G. C., Wunch, D., Roehl, C. M., Wennberg, P. O., Griffith, D. W. T., Deutscher, N. M., Warneke, T., Notholt, J., Robinson, J., Sherlock, V., Connor, B., Rettinger, M., Sussmann, R., Ahonen, P., Heikkinen, P., Kyrö, E., Mendonca, J., Strong, K., Hase, F., Dohe, S., and Yokota, T.: Improvement of the retrieval algorithm for GOSAT SWIRXCO₂ and XCH₄ and their validation using TCCON data, *Atmos. Meas. Tech.*, 6, 1533-1547, doi:10.5194/amt-6-1533-2013, 2013.
- Yan, X., Akiyama, H., Yagi, K., and Akimoto, H.: Global estimations of the inventory and mitigation potential of methane emissions from rice cultivation conducted using the 2006 Intergovernmental Panel on Climate Change Guidelines, *Global Biogeochem. Cycles*, 23, GB2002, doi:10.1029/2008GB003299, 2009.
- Zou, M., Xiong, X., Saitoh, N., Warner, J., Zhang, Y., Chen, L., Weng, F., and Fan, M.: Satellite observation of atmospheric methane: intercomparison between AIRS and GOSAT TANSO-FTS retrievals, *Atmos. Meas. Tech.*, 9, 3567-3576, doi:10.5194/amt-9-3567-2016, 2016.

Figures.

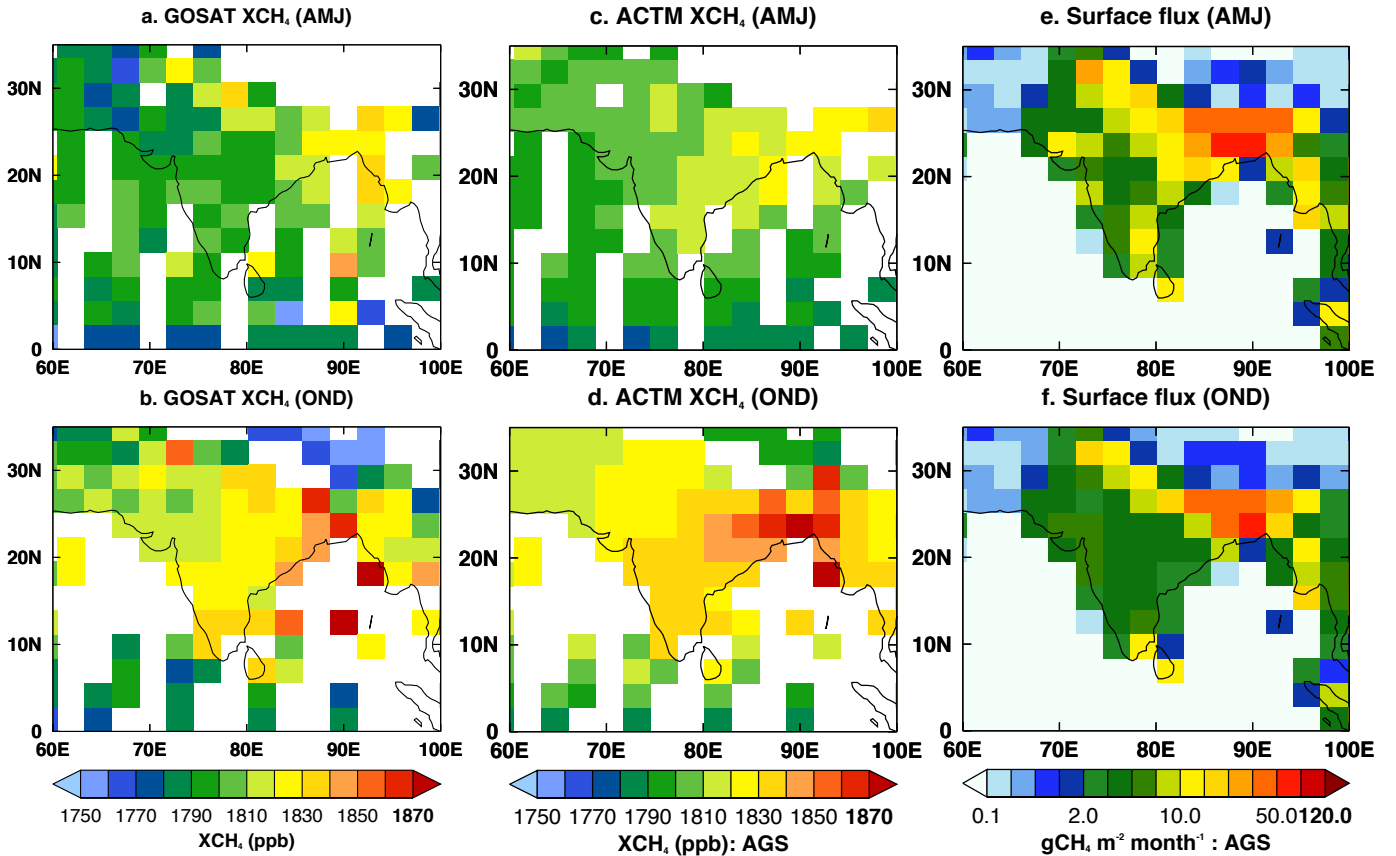


Figure 1: Average seasonal distributions (from 2011 to 2014) of XCH_4 obtained from GOSAT observations (a-b), ACTM simulations (c-d) and CH_4 emission consisting of all the natural and anthropogenic emissions (e-f: ACTM_AGS case) over the Indian region. Optimized emissions are shown from a global inversion of surface CH_4 concentrations (Patra et al., 2016) and multiplied by a constant factor of 12 for a clear visualization. The ACTM is first sampled at the location and time of GOSAT observations and then seasonally averaged. The white spaces in panels (a-d) are due to the missing data caused by satellite retrieval limitations from cloud cover.

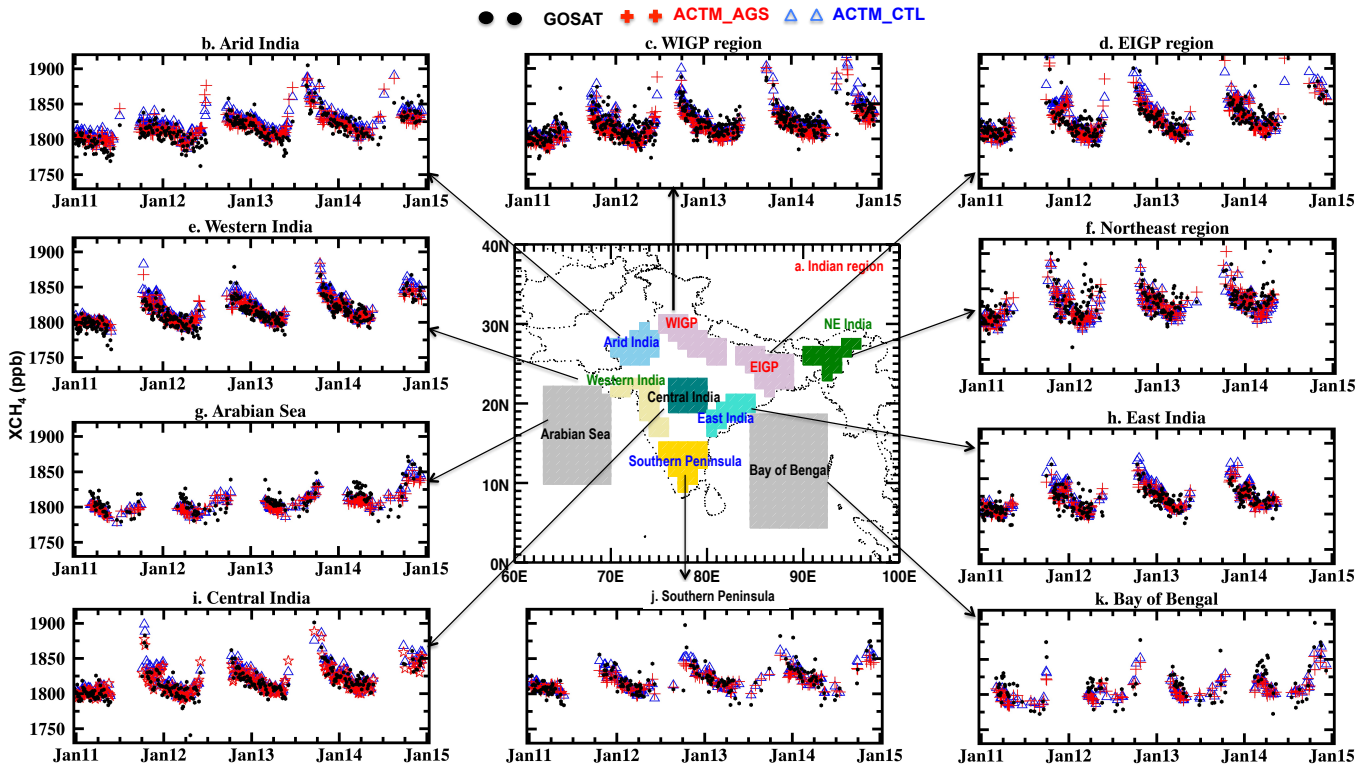


Figure 2: (a) The map of the regional divisions (shaded) for the time series analysis. (b-l) Time series of XCH₄ over the selected regions (shown in map) as obtained from GOSAT and simulated by ACTM for two different emission scenarios, namely, ACTM_ags and ACTM_ctl. The gaps are due to the missing observational data.

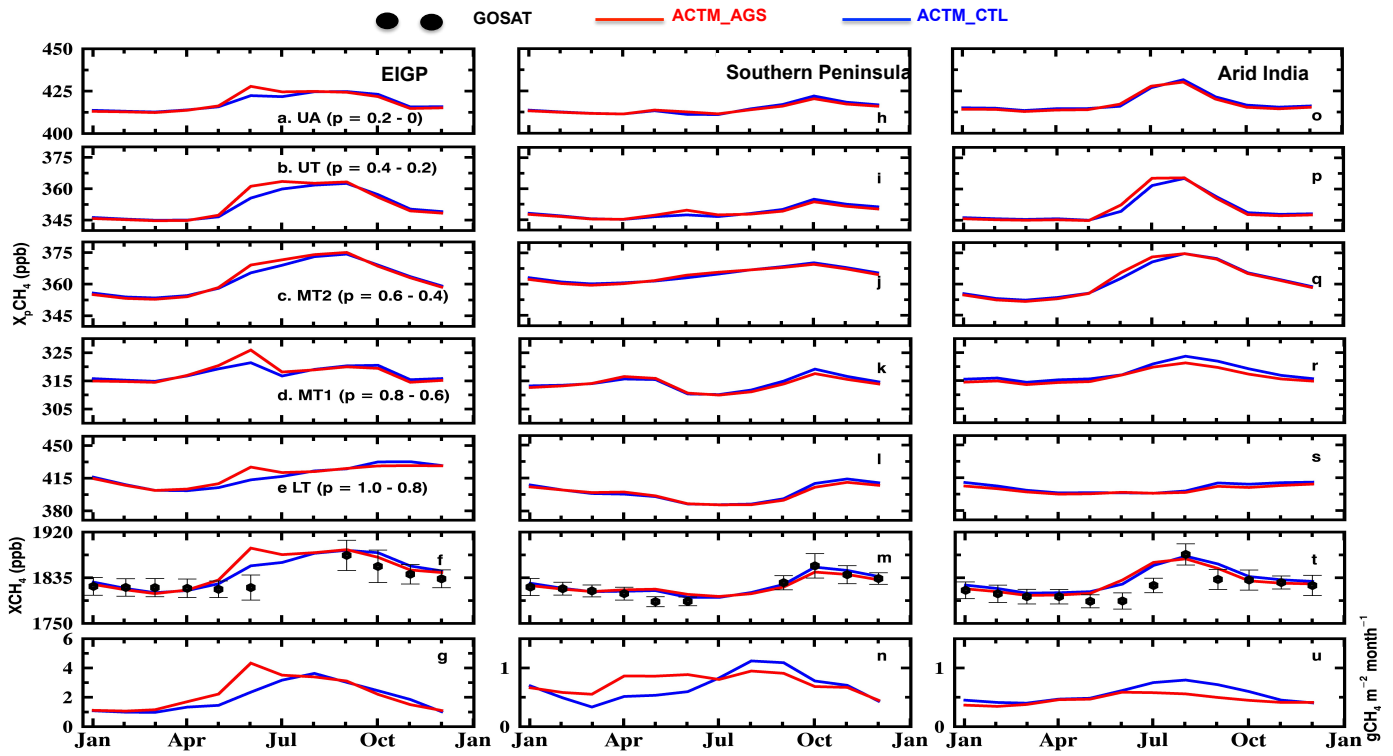


Figure 3: The bottom panels show the monthly mean climatology of the total optimized CH_4 emissions (panels g, n, u); estimated after performing the global inverse analysis (Patra et al., 2016). The second bottom panels show $X\text{CH}_4$ obtained from the GOSAT observations (black circles in panels f, m, t) and ACTM simulations (panels f, m, t) over the Eastern IGP (first column), Southern Peninsula (second column) and Arid India region (third column). Monthly climatology is based on the monthly mean values for the period of 2011-2014 for all the values. The error bars in the GOSAT monthly mean values depict the 1-sigma standard deviations for the corresponding months (f, m, t). The 1-sigma values are not plotted for the model simulations to maintain figure clarity. Simulations are based on two different emission scenarios namely ACTM_CTL (blue lines) and ACTM_AGS (red lines) based on the different combinations of emissions. The upper five panels show the monthly climatology of partial columnar methane (denoted by $X_p\text{CH}_4$) calculated at five different partial sigma-pressure layers; 1.0-0.8 (e, l, s), 0.8-0.6 (d, k, r), 0.6-0.4 (c, j, q), 0.4-0.2 (b, i, p) and 0.2-0.0 (a, h, n). Please note that the y scales in the emission plots over southern peninsula and Arid India (n and u) are different from over the EIGP region (g).

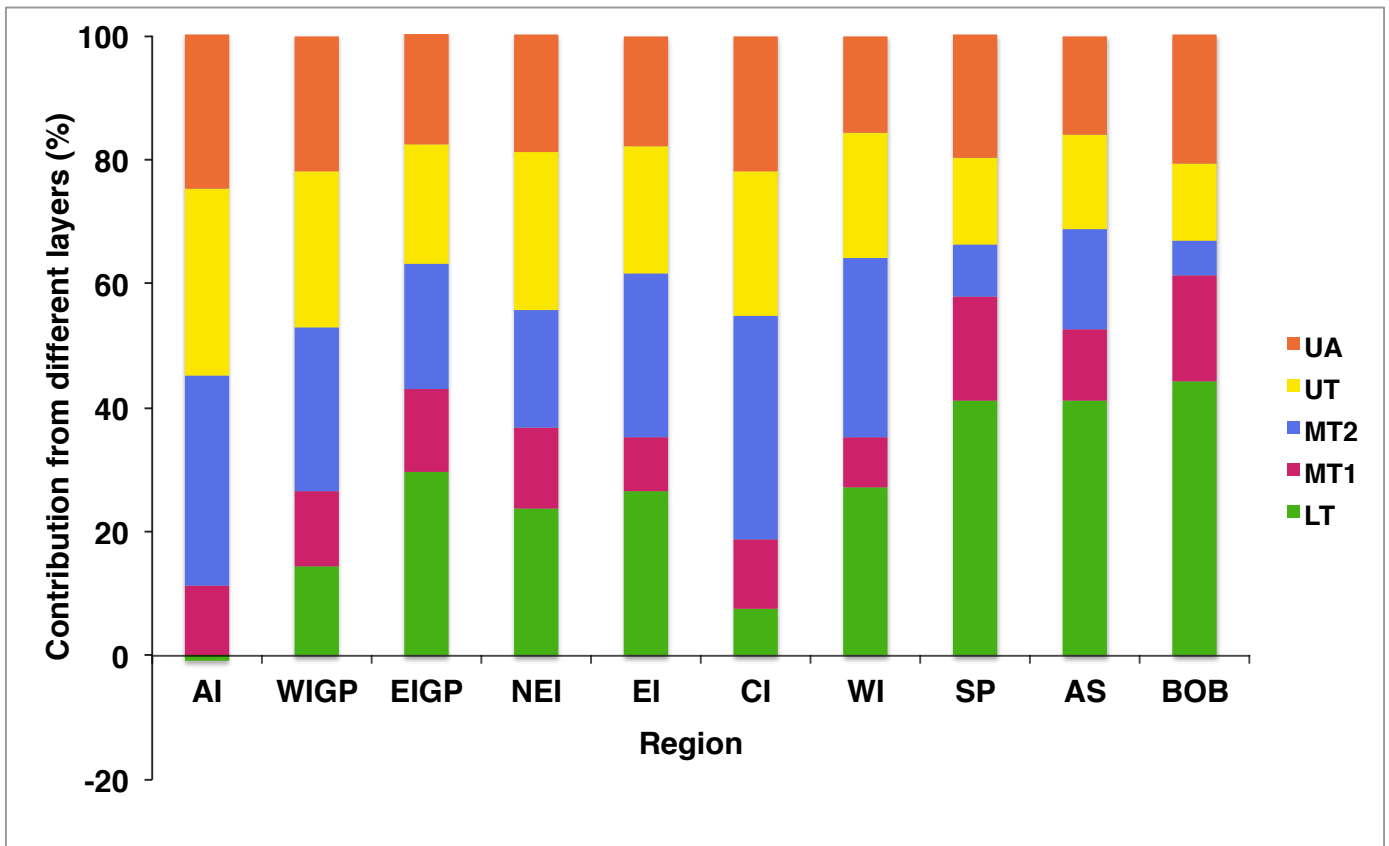


Figure 4: Contributions of partial columns in the seasonal amplitude of XCH_4 over selected regions for AGS case. Differences in the X_pCH_4 , calculated at the same time as the maxima and minima of the seasonal XCH_4 cycle, are used to calculate the percentage contributions of respective partial columns in the seasonal amplitude of XCH_4 .

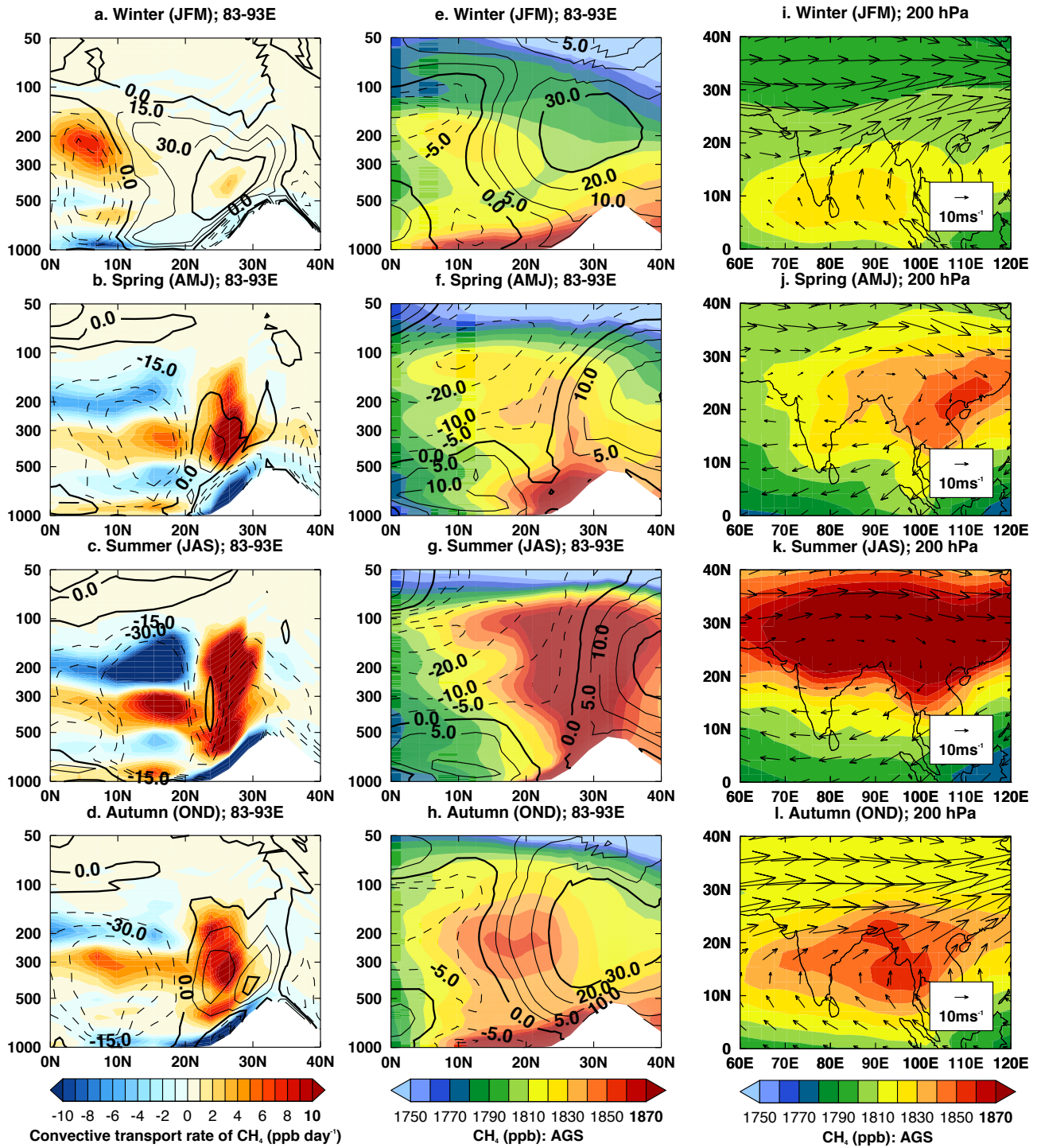


Figure 5: Vertical structure of seasonally averaged CH_4 transport rate due to the convection (a-d, in ppb day^{-1}) and CH_4 mixing ratios (e-h from AGS scenarios) averaged over 83-93°E for the year 2011. Positive and negative transport rate values represent the accumulation and dissipation of mass, respectively. The contour lines in the first (a-d) and second (e-h) columns depict the average omega velocity (in hPa s^{-1}) and u wind component, respectively for the same period. The solid contour lines show the positive values and dotted lines show negative values. Positive and negative values of the omega velocity represent downward and upward motions, respectively. The zero value of u wind shows wind is pure either southerly or northerly. White spaces in

513 zonal-mean plots (a- h) show the missing data due to orography. The rightmost column depicts the maps of averaged CH₄ and
514 wind vectors (in m s⁻¹; arrow) during all the four seasons in 2011 at 200 hPa height (i-l).